version of August 23, 2015

INTERNSHIP REPORT
Hydrodynamic simulations of rotating black holes

Antoine BOULET[†]

ABSTRACT – The analogue gravity consists to study phenomenon from general relativity through other physical systems using waves in fluid flow, Bose-Einstein condensate or superfluid helium for instance.
The experiments relying on the analogy between black holes and fluid dynamics physic are very fruitfully to study, understand and constrain models of classical and quantum field theory in curved space-time. The real advantage of these experiments is that they can be reproduced in a laboratory.
In this report, we first present some aspect of black holes physics, and its link with fluid mechanics. In particular we focus on a phenomenon occurring in the vicinity of rotating black holes holes, *i.e.* superradiance the mechanism that allows rotating black holes to lose their angular momentum. Then we explore an optical method to observe superradiant scattering in our analogue gravity system, *i.e.* surface waves on stationary draining fluid flows.
The detection method under consideration is Fourier Transform Profilometry (FTP). This method consists to project a periodic pattern on an object, and using a Fourier transform of the signal, we can reconstruct, with great accuracy and without disturbing the deformation, amplitude of the object compared to a reference plan. In fact, the deformation (that is to say, the object) introduce a shift in the phase of the Fourier transform and this phase is directly correlated to the amplitude of the deformation. A major part of this presentation is devoted to the study of the FTP method. Theoretical limitations are found, as well as the ideal parameters an the experimental set-up. We present several key results related to the accuracy of the FTP method obtained from numerical studies, and discuss experimental challenges to overcome when used in the experiment.

Keywords: classical and quantum field theory in curved space-times, analogue gravity, black hole, fluid mechanic, superradiance, Fourier transform profilometry.

Internship carried out during the fundamental physics academic training (second year of magisterium) offered by Paris-Sud University[a] from May 18, 2015 to August 16, 2015 at Quantum Gravity Laboratory[b], Univerity of Nottingham, under the supervision of Silke WEINFURTNER [‡].

[†]Antoine BOULET
Paris-Sud University;
Magisterium of fundamental physics;
antoine.boulet@u-psud.fr

[‡] Silke WEINFURTNER
Universtiy of Nottingham;
Quantum Gravity Laboratory;
silke.weinfurtner@nottingham.ac.uk

[a]Magisterium of fundamental physics, Paris-Sud University, 91405 Orsay Cedex, France. Web site: http://www.magistere.u-psud.fr/

[b]Mathematical Sciences Building, University Park, Nottingham, NG7 2RD, United Kingdom. Web site: http://www.gravitylaboratory.com/

Contents

Acknowledgement

I would like to thank Silke Weinfurtner, my supervisor, for her kindness, her generosity, her welcome, her goodwill, and her continuous effort to to encourage me to communicate despite my poor English. Thank you Silke.

Thanks too my colleagues with who I shared the Quantum Gravity Fluid Laboratory: Andrew Scoins, Daniel Goodfellow, Henry Tanner (sait “monsieur trés bien”) and Zack Fifer (said “the freak”). They allowed a friendly atmosphere in the laboratory. Special thanks to Zack for his help with my English.

Finally, I thank the university of Paris-Sud and the university of Nottingham for their support.

Introduction

In 1974, Hawking predicted 'Black holes explosions' and the radiation of black holes [1, 2]. Although nothing can escape the horizons of black holes according to classical theory of the general relativity, it seems that considering the quantum physics, black holes black holes emit black body radiation, with a temperature proportional to the inverse of their mass. This prediction encounters the trans-Plankian problem [3, 4]: the Hawking photons observed would have wavelengths smaller than the Plank-length near black holes and it is expected that quantum gravity effects are significant. Since we have no quantum gravity theory, trans-Plankian effects could modify – or even suppress – Hawking radiation.

Because of the distance between black holes and us combined to the smallness of phenomenon compared to the gravitational/cosmological effects (*e.g.* the Hawking temperatures of black holes are very small compared to the temperature of the cosmic microwave background), it seems impossible to directly detect Hawking radiation form astrophysical black holes. One way to overcome this problem, is to use analogue gravity systems to experimentally probe our theoretical models for quantum field theory in curved spacetimes [5]. Considering only the hydrodynamic equation for a perfect irroational barotropic fluid, sound/surface waves in a fluid flows exceeding the speed of sound/surface waves can encounter an acoustic horizons[1], and thus share some of the same behaviour of photons near black holes. In this analogue system, the velocity of sound is analogous to the velocity of light, and the Plank-length is replaced by the distance of the water molecules. Therefore, the study of analogue systems should be a guide to test the robustness of various classical and quantum field theories.

In this internship I helped with the preparation of an experiment on analogue rotating black holes. A major part of the experiment is related with the observation of superradiant scattering of surface waves with bathtub vortex flows. In particular, the experimental challenge is to employ optical techniques to accurately measure the free surface (containing all surface waves) of the bathtub vortex flow. In section 1 we present the basic theories to understand analogy between black holes and fluid mechanics and the phenomenon of superradiance. In section 2 we present the experiment, an optical profilometry method, the parameter search of the profilometry method for the experimental setup and the results of the numerical simulations.

1 A bit of theory

1.1 Analogue gravity in fluid systems

In this section we show the analogy between small perturbations in fluid flows and classical and quantum field theory in curved spacetimes. We closely follow the original derivation by Unruh published in 1981 [5].

A classical fluid can be described in each point in space by: its density ρ, its pressure p and its velocity $\boldsymbol{v}$. Assuming an inviscid and irrotational fluid, *i.e.* $\boldsymbol{\nabla} \times \boldsymbol{v} = 0$, we define ψ such as $\boldsymbol{v} = \boldsymbol{\nabla}\psi$. We also assume that p is a function of ρ through the equation of state (barotropic fluid, *e.g.* isothermal fluid). In this case Navier-Stockes equations are reduced to Euler equations (1) and continuity equation (2):

$$\frac{\partial \boldsymbol{v}}{\partial t} + (\boldsymbol{v}\cdot\boldsymbol{\nabla})\,\boldsymbol{v} = -\frac{1}{\rho}\boldsymbol{\nabla}p - \boldsymbol{\nabla}\phi \quad \Rightarrow \quad \left(\frac{\partial}{\partial t} + (\boldsymbol{\nabla}\psi\cdot\boldsymbol{\nabla})\right)\boldsymbol{\nabla}\psi = -\frac{1}{\rho}\boldsymbol{\nabla}p - \boldsymbol{\nabla}\phi \tag{1}$$

$$\frac{\partial \rho}{\partial t} + \boldsymbol{\nabla}\cdot\rho\boldsymbol{v} = 0 \quad \Rightarrow \quad \frac{\partial \rho}{\partial t} + \boldsymbol{\nabla}\cdot(\rho\boldsymbol{\nabla}\psi) = 0 \tag{2}$$

where ϕ is the external force potential. Then with vector calculus identities, we have:

$$\frac{1}{2}\boldsymbol{\nabla}\boldsymbol{v}\cdot\boldsymbol{v} = (\boldsymbol{v}\cdot\boldsymbol{\nabla})\,\boldsymbol{v} + \boldsymbol{v}\times(\boldsymbol{\nabla}\times\boldsymbol{v})$$

and, because the fluid is irrotational (*i.e.* $\boldsymbol{\nabla}\times\boldsymbol{v} = 0$), equation (1) become

$$\frac{\partial\boldsymbol{\nabla}\psi}{\partial t} + \frac{1}{2}\boldsymbol{\nabla}\left((\boldsymbol{\nabla}\psi)^2\right) = -\frac{1}{\rho}\boldsymbol{\nabla}p - \boldsymbol{\nabla}\phi \tag{1.a}$$

Then we integrate the equation (1.a):

$$\begin{aligned}\frac{\partial\psi}{\partial t} + \frac{1}{2}(\boldsymbol{\nabla}\psi)^2 + \phi &= -\int\frac{1}{\rho}\boldsymbol{\nabla}p\,\mathrm{d}\boldsymbol{r} + K \\ &= -\int^{\rho}\frac{1}{\rho'}\frac{\mathrm{d}p}{\mathrm{d}\rho'}\,\mathrm{d}\rho' + K\end{aligned} \tag{1.b}$$

where K is the constant of the integration.

[1] An acoustic horizon define two regions in the fluid: the first where velocity of fluid is lower to velocity of sound and the second where velocity of fluid is superior to velocity of sound (acoustic black hole)

Now, we do a change of variables:

$$\xi \equiv \ln \rho \qquad f(\xi) \equiv \int^{\rho} \frac{1}{\rho'} \frac{\mathrm{d}p}{\mathrm{d}\rho'} \, \mathrm{d}\rho'$$

and equation (2) become:

$$\frac{\partial \xi}{\partial t} \frac{\mathrm{d}\mathrm{e}^{\xi}}{\mathrm{d}\xi} + \boldsymbol{\nabla}\psi \cdot \boldsymbol{\nabla}\mathrm{e}^{\xi} + \mathrm{e}^{\xi}\boldsymbol{\nabla}^2\psi = 0 \qquad \Rightarrow \qquad \frac{\partial \xi}{\partial t} + \boldsymbol{v} \cdot \boldsymbol{\nabla}\xi + \boldsymbol{\nabla} \cdot \boldsymbol{v} = 0 \tag{2.a}$$

We linearise equations (1.b) and (2.a), where we decompose $\rho \equiv \rho_0 + \delta\rho$ (as far as $\boldsymbol{v}$, ξ and ψ); $\{\rho_0, \boldsymbol{v_0}\}$ is a solution of equations (1) and (2) with $\delta\rho \ll \rho_0$ an perturbation.

We obtain

$$\text{order 0} \qquad \frac{\partial \psi_0}{\partial t} + \frac{1}{2}{v_0}^2 + \phi = -f(\xi_0) + K \tag{1.c}$$

$$\frac{\partial \xi_0}{\partial t} + \boldsymbol{v_0} \cdot \boldsymbol{\nabla}\xi_0 + \boldsymbol{\nabla} \cdot \boldsymbol{v_0} = 0 \tag{2.b}$$

$$\text{order 1} \qquad \frac{\partial\, \delta\psi}{\partial t} + \boldsymbol{v_0} \cdot \delta\boldsymbol{v} + f'(\xi_0)\, \delta\xi = 0 \qquad \Rightarrow \qquad \delta\xi = -\frac{1}{f'(\xi_0)} \left(\frac{\partial\, \delta\psi}{\partial t} + \boldsymbol{v_0} \cdot \delta\boldsymbol{v} \right) \tag{1.d}$$

$$\frac{\partial\, \delta\xi}{\partial t} + \boldsymbol{v_0} \cdot \boldsymbol{\nabla}\, \delta\xi + \delta\boldsymbol{v} \cdot \boldsymbol{\nabla}\xi_0 + \boldsymbol{\nabla} \cdot \delta\boldsymbol{v} = 0 \tag{2.c}$$

Then, using relation $\boldsymbol{\nabla} \cdot \delta\xi\boldsymbol{v_0} = \delta\xi\boldsymbol{\nabla} \cdot \boldsymbol{v_0} + \boldsymbol{v_0} \cdot \boldsymbol{\nabla}\, \delta\xi$ in equation (2.c), we have

$$\frac{\partial\, \delta\xi}{\partial t} + \boldsymbol{\nabla} \cdot \delta\xi\boldsymbol{v_0} + \delta\boldsymbol{v} \cdot \boldsymbol{\nabla}\xi_0 + \boldsymbol{\nabla} \cdot \delta\boldsymbol{v} = \delta\xi\boldsymbol{\nabla} \cdot \boldsymbol{v_0} \tag{2.d}$$

Noting that

$$\begin{aligned} \frac{1}{\rho_0}\boldsymbol{\nabla} \cdot \rho_0\, \delta\boldsymbol{v} &= \delta\boldsymbol{v}\frac{\boldsymbol{\nabla}\rho_0}{\rho_0} + \boldsymbol{\nabla} \cdot \delta\boldsymbol{v} \\ &= \delta\boldsymbol{v}\boldsymbol{\nabla}\xi_0 + \boldsymbol{\nabla} \cdot \delta\boldsymbol{v} \end{aligned}$$

and, using equation (2),

$$\begin{aligned} \frac{\partial \rho_0\, \delta\xi}{\partial t} + \boldsymbol{\nabla} \cdot \delta\xi\rho_0\boldsymbol{v_0} &= \rho_0 \left(\frac{\partial\, \delta\xi}{\partial t} + \boldsymbol{\nabla} \cdot \delta\xi\boldsymbol{v_0} \right) + \left(\frac{\partial \rho_0}{\partial t} + \boldsymbol{\nabla} \cdot \rho_0\boldsymbol{v_0} \right) \delta\xi \\ &= \rho_0 \left(\frac{\partial\, \delta\xi}{\partial t} + \boldsymbol{\nabla} \cdot \delta\xi\boldsymbol{v_0} \right) \end{aligned}$$

equation (2.d) become

$$\frac{1}{\rho_0} \left(\frac{\partial \rho_0\, \delta\xi}{\partial t} + \boldsymbol{\nabla} \cdot (\rho_0\boldsymbol{v_0}\, \delta\xi) + \boldsymbol{\nabla} \cdot \rho_0\, \delta\boldsymbol{v} \right) = \delta\xi\boldsymbol{\nabla} \cdot \boldsymbol{v_0} \tag{2.e}$$

Finally after some manipulations (we replace $\delta\xi$ in equation (2.e) with equation (1.d)), we obtain an equation for $\delta\psi$:

$$\frac{\partial}{\partial t} \left(\frac{\rho_0}{c_s} \frac{\partial\, \delta\psi}{\partial t} \right) + \frac{\partial}{\partial t} \left(\frac{\rho_0}{c_s} \boldsymbol{v_0} \cdot \boldsymbol{\nabla}\, \delta\psi \right) + \boldsymbol{\nabla} \cdot \left(\frac{\rho_0\boldsymbol{v}}{c_s} \frac{\partial\, \delta\psi}{\partial t} \right) + \boldsymbol{\nabla} \cdot \left(-\rho_0\boldsymbol{\nabla}\, \delta\psi + \frac{\rho_0\boldsymbol{v}}{c_s} (\boldsymbol{v_0} \cdot \boldsymbol{\nabla}\, \delta\psi) \right) = 0 \tag{3}$$

where we note $c_s = f'(\xi_0)$, the local velocity of the sound (in the following, we assume that this quantity is constant[2]).

Scharzschild astrophysical black holes

The gravitational field, the metric $g^{\mu\nu}$, is solution of the Einstein's equations which link the geometry of the spacetime and its material content. The metric is defined by the local relativistic invariant

$$\mathrm{d}s^2 = g_{\mu\nu}(x^{\lambda})\, \mathrm{d}x^{\mu}\, \mathrm{d}x^{\nu}$$

and, for example near the horizon of Schwarzschild black holes[3] with mass M we have [6]

$$\mathrm{d}s^2 \underset{\tilde{r}/r_s \to 1^+}{\simeq} -\left(1 - \frac{\tilde{r}}{r_s}\right) \mathrm{d}\tilde{t}^2 + \left(1 - \frac{\tilde{r}}{r_s}\right)^{-1} \mathrm{d}\tilde{r}^2 \tag{4}$$

where $\tilde{t}$ and $\tilde{r}$ are the time and the radial space coordinates respectively and $r_s = 2GM/c^4$ (c is the speed of light).

[2] Available for an incompressible fluid ($\boldsymbol{\nabla} \cdot \boldsymbol{v} = 0$).

[3] The Schwarzschild's black holes are uncharged black hole without angular momentum. Remark: black holes are only defined by their mass, charge and angular momentum (no hair theorem [6, 2]).

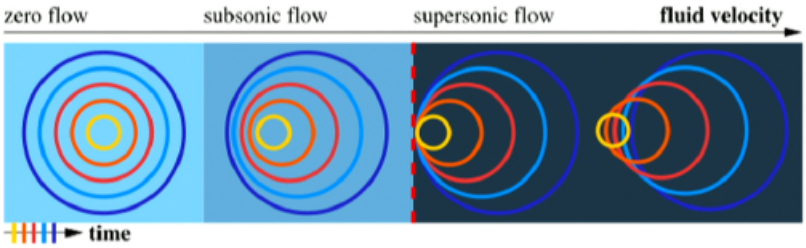

Figure 1: Acoustic horizons. This figure has been taken from [8]. The propagation of sound waves in a convergent fluid flow exhibiting subsonic and supersonic flow regions are depicted. The dashed red lines, separating the subsonic and supersonic regions, indicate the location of the acoustic black horizon.

Field theory in curved spacetimes

For a geometry encoded in the metric $g^{\mu\nu}$, the equation of motion for massless particles, described by the scalar field Ψ, is [7]:

$$\left(\frac{1}{\sqrt{-g}}\partial_\mu\sqrt{-g}g^{\mu\nu}\partial_\nu\right)\Psi = 0 \tag{5}$$

where $g = \det g_{\mu\nu}$.

Analogue gravity

Combining equations (3) and (5), we obtain

$$\sqrt{-g}g^{tt} = \frac{\rho_0}{{c_s}^2} \qquad \sqrt{-g}g^{ti} = \sqrt{-g}g^{it} = -\frac{\rho_0}{{c_s}^2}{v_0}^i \qquad \sqrt{-g}g^{ij} = -\rho_0\delta^{ij} + \frac{\rho_0}{{c_s}^2}{v_0}^i{v_0}^j$$

hence the analogue metric for phonons $\delta\psi$:

$$\mathrm{d}s^2 = \frac{\rho_0}{c_s}\left(({c_s}^2 - \boldsymbol{v_0}\cdot\boldsymbol{v_0})\,\mathrm{d}t^2 + 2\,\mathrm{d}t\boldsymbol{v_0}\cdot\mathrm{d}\boldsymbol{x} - \mathrm{d}\boldsymbol{x}\cdot\mathrm{d}\boldsymbol{x}\right) \tag{6}$$

This becomes, assuming spherical symmetry (with $v_0 < 0$) and the stationary of the fluid flow[4],

$$\mathrm{d}s^2 = \frac{\rho_0}{c_s}\left(({c_s}^2 - {v_0}^2)\,\mathrm{d}t^2 - \frac{c_s}{{c_s}^2 - {v_0}^2}\,\mathrm{d}r^2 - r^2\left(\mathrm{d}\theta^2 + \sin^2\theta\,\mathrm{d}\varphi^2\right)\right) \tag{7}$$

Now, if we assume $v_0 = -c_s + \alpha\,(r - R)$ – since near the horizon, the velocity of the fluid is equal to the velocity of the sound –, where α and R (the radius of analogue horizon) are positive constants, we obtain

$$\mathrm{d}s^2 \underset{r/R\to 1^+}{\simeq} \frac{\rho_0}{c_s}\left(-2c_s\alpha R\left(1 - \frac{r}{R}\right)\mathrm{d}t^2 + \frac{1}{2\alpha R}\left(1 - \frac{r}{R}\right)^{-1}\mathrm{d}r^2\right) \tag{8}$$

an equivalent metric to Scharzschild black holes compared to equation (4).

Therefore we see that the phonons of the fluid obey the same equations of motion as the photons near the horizon of black holes. It is possible to create a fluid system which reproduces an analogue geometry in a classical fluid: the zone where the velocity of the fluid is superior to the velocity of waves can be seen as black holes because, if the fluid has greater speed than the sound, no waves can escape of the acoustic black holes (see figure 1).

1.2 Superradiant scattering

The previous discussion consider the phonons of fluid, but the analogy can be introduce considering the surface waves (see [9] for details): in this case, the velocity of the sound is replaced by the velocity of the surface waves[5], and the small deformations of the surfaces waves play the role of the photons near the black holes. In fact we can have event horizon for the surface waves. The real advantage to use surface waves is that it is easier to obtain effective analogue event horizon: sound waves require a flow with velocity reaching $c_s \sim 10^3$ m.s^{-1}, this type of horizon require a flow with velocity $\sim 10^0$ m.s^{-1}.

[4]These assumptions are non-realist in 3 spacial dimensions (because of conservation of mass and finite compressibility), but we can imagine model in 2 dimensions with a vortex.

[5]See for example exercise of Frederic Moisy about surface waves (in french): dispersive relation of gravity waves in shallow water (where the surface tension is neglected) is $\omega^2 = gk\tanh(kh)$; hence, velocity of wave is given by $c_h \sim \sqrt{gh}$, for $kh \ll 1$; and, for $kh \gg 1$, $k \sim \omega/\sqrt{g}$.

The Hawking radiation is an effect which require introduction of quantum field theory, the creation of pair particle-antiparticles in a spacetimes geometry; it is a quantum effect where the black holes emit radiation. But there exist a similar properties, that is to say the emission of particles by another process: superradiant scattering. This phenomenon appear when waves with frequency ω and azimuthal number m are in incidence on a rotating black hole with angular velocity at the black hole horizon Ω_{BH}. Near the horizon, the waves undergo an effective potential in the equation of motion for massless scalar particle [10, 11]. That is to say, equation (5) is equivalent to $(\partial^\nu \partial_\nu + V)\,\Psi = 0$, an equation where particles undergoes an effective potential V. If the supperadiance condition is checked ($\omega - m\Omega_{BH} < 0$), the incident waves are amplified after the reflection on the event horizon [10, 12].

This process is, of course, also relevant for the analogue systems as our experiment. The major aim is to detect an amplification of the reflected surface waves on the analogue event horizon. In an realistic experimental set up, surface waves should be amplified by a factor ~ 1.1 (see [13] for details). In our experiment we create incident surface waves with ~ 1 mm of amplitude in order to stay in the linear regime[5].

One of the difficulties in detecting superradiant scattering is to measure, with great accuracy, the surface waves amplification without destroy it. This project was devoted to test numerically one used method to detect deformations in surfaces (see the following section 2.1), which we intend, in the future, to apply to the free surface in our experimental set-up.

2 Analysis of Fourier Transform Profilometry (FTP)

2.1 Profilometry by Fourier transform

Now, we present a method which permits us to detect the superradiant waves on the water suface: profilometry by Fourier transform. This methodology is taken in major part from Takeda's paper [14].

The idea relies on the utilisation of a periodic light pattern projected on a surface (*e.g.* water) which is distorted by deformation (*e.g.* surface waves) of the free surface (see figure 2). Since the grating image on

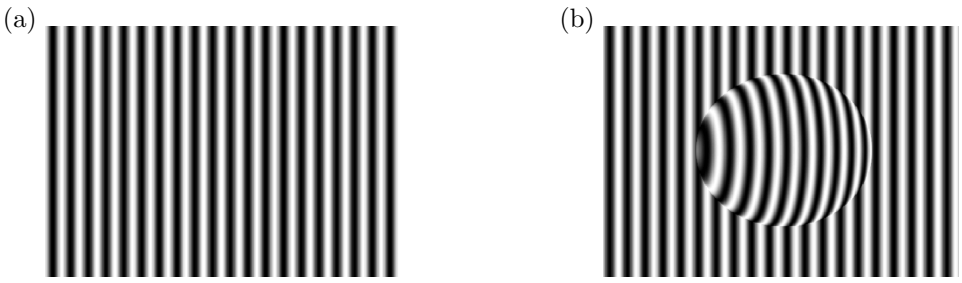

Figure 2: Profilometry principle. (a) Reference fringe pattern projected on free surface; (b) deformed fringe by deformation on free surface.

the flat surface is periodic (along x-axis), with frequency denoted f_0, the intensity of the projected image and sensed by the camera can be decomposed in Fourier series:

$$I_0(x,y) = \sum_{n=-\infty}^{\infty} A_n \mathrm{e}^{\mathrm{i}nkx} \mathrm{e}^{\mathrm{i}n\phi_0(x,y)} \tag{9}$$

where $k \equiv 2\pi f_0$ and ϕ_0 encode the pattern. We assume the optical axis of the projector and the camera are normal to the free surface and, by simple geometrics assumptions, we show that (see section 2.2 for detail), for a deformation $z = s(x,y)$, the signal measured by the camera can be expanded as:

$$I(x,y) = r(x,y) \sum_{n=-\infty}^{\infty} A_n \mathrm{e}^{\mathrm{i}nkx} \mathrm{e}^{\mathrm{i}n\phi(x,y)} \tag{10}$$

where r is the distribution of reflectivity on the deformed surface and ϕ encodes the deformation s – which depends only on the position between the surface and the sensors (*e.g.* camera). In the ideal case, $\Delta\phi \equiv \phi - \phi_0 \propto s$ (see equation (25) of section 2.2).

Now, we select the first harmonic in the Fourier spectrum, denoted $\hat{I}_0 \equiv A_1 \exp(\mathrm{i}kx)\exp(\mathrm{i}\phi_0)$ and $\hat{I} \equiv rA_1 \exp(\mathrm{i}kx)\exp(\mathrm{i}\phi)$ for I_0 and I respectively. Then:

$$\mathrm{Im}\left(\log \hat{I}\hat{I}_0^{\,*}\right) = \Delta\phi \tag{11}$$

Remark: We use the complex logarithm, thus $\Delta\phi \in [0, 2\pi]$ *thought* $s \in [s_{\min}, s_{\max}]$ *is continuous; it is necessary to take into consideration this aspect with a multi-valued function in order to correct the discontinuity of* $\Delta\phi$*, see* e.g. *[15].*

Finally, this method permits us to detect (in theory) the surface waves and, together with computing and video acquisition, we can study the propagation of superradiant phonons near the acoustic rotating black hole horizons.

2.2 Virtual simulation of 3D objects using ray-tracing techniques

To test the limit and accuracy of the FTP method, it was necessary to be able to have a scenario where the instrumental set-up can be idealised. By considering the geometry of our proposed set-up, it was possible to generate virtual images (as seen by a camera) in MATLAB. Suppose we have a surface on the plane $z = \lambda$ where λ is constant. We note the following points (see figure 3):

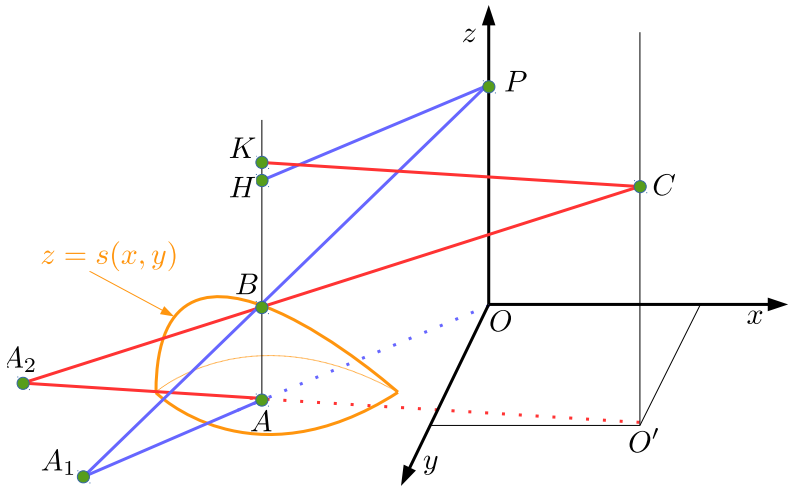

Figure 3: The setup of the experiment. The projector P projects a pattern I_0 on the plane $z = \lambda = 0$ and the camera C receives an intensity I due to the object surface.

P - Projector, with coordinates (x_p, y_p, z_p);

C - Camera, with coordinates (x_c, y_c, z_c);

B - A point on the object surface, with coordinates $(x, y, \lambda + s(x, y))$;

A - An orthogonal projection of B on the plane $z = \lambda$, with coordinates (x, y, λ);

A_1 - Point on the plane $z = \lambda$ which is a continuation of the ray from P to B, with coordinates (x_1, y_1, λ);

A_2 - Point on the plane $z = \lambda$ which is a continuation of the ray from C to B, with coordinates (x_2, y_2, λ);

H - An orthogonal projection of P, which is orthogonal to the plane $z = \lambda$ and the point B, with coordinates (x, y, z_p);

K - An orthogonal projection of C, which is orthogonal to the plane $z = \lambda$ and the point B, with coordinates (x, y, z_c);

O - An orthogonal projection of P on the plane $z = \lambda$, with coordinates (x_p, y_p, λ);

O' - An orthogonal projection of C on the plane $z = \lambda$, with coordinates (x_c, y_c, λ)

By considering the geometry, we have the following relation:

$$I(x_2, y_2) = r(x, y) I_0(x_1, y_1) \tag{12}$$

Furthermore, we assume that each point of the object surface is accessible by the light rays coming from from P, and that each point can be viewed by C (no shadowing). Now assuming that the dimensions of plane l_ι intercepted by the camera (and by the projector) $[-l_x, l_x] \times [-l_y, l_y]$ are equivalent, this condition is equivalent to:

$$\forall (x, y) \in [-l_x, l_x] \times [-l_y, l_y], \qquad \left|\frac{\partial s}{\partial x}\right| \leq \left|\frac{s - z_\iota}{x - x_\iota}\right| \quad \text{and} \quad \left|\frac{\partial s}{\partial y}\right| \leq \left|\frac{s - z_\iota}{y - y_\iota}\right|$$

Finally, the aim is to find x_1, x_2, y_1 and y_2 as a function of the coordinates of B, P and C. To do this we need four independent equations. We can use the fact that the triangle A_1BA (respectively A_2BA) is homothetic of triangles A_1PO and BHP (respectively A_2CO' and BKC), thus we have:

$$\left|\frac{A_1A}{PH}\right| = \left|\frac{AB}{BH}\right| \qquad \left|\frac{A_2A}{CK}\right| = \left|\frac{AB}{BK}\right| \qquad \left|\frac{AB}{A_1A}\right| = \left|\frac{PO}{A_1O}\right| \qquad \left|\frac{AB}{A_2A}\right| = \left|\frac{CO'}{A_2O'}\right|$$

Remark: In the following, we enforce the arbitrary choice of the coordinates origin at $O = (x_p, y_p, \lambda) = (0, 0, 0)$ *such that* $s \geq 0$ *and the direction of axis such that* $z_\iota > 0$.

2.2.1 Algebraic solution

Substituting the coordinates of the points into these equations, we obtain

$$F_p{}^2 = (x_1 - x)^2 + (y_1 - y)^2 \tag{13}$$
$$F_c{}^2 = (x_2 - x)^2 + (y_2 - y)^2 \tag{14}$$
$$G_p{}^2 = (x_1 - x_p)^2 + (y_1 - y_p)^2 \tag{15}$$
$$G_c{}^2 = (x_2 - x_c)^2 + (y_2 - y_c)^2 \tag{16}$$

where we noted[6]

$$\mathcal{I}_\iota \equiv \sqrt{(x_\iota - x)^2 + (y_\iota - y)^2} \qquad F_\iota \equiv \frac{s}{z_\iota - s}\mathcal{I}_\iota \qquad G_\iota \equiv \frac{z_\iota}{z_\iota - s}\mathcal{I}_\iota$$

To solve this system, we change parametrization and we introduce four angles α_ι and β_ι defined by

$$\begin{array}{rclrcl} F_p\cos\alpha_p &\equiv& x_1 - x & F_p\sin\alpha_p &\equiv& y_1 - y \\ F_c\cos\alpha_c &\equiv& x_2 - x & F_c\sin\alpha_c &\equiv& y_2 - y \\ G_p\cos\beta_p &\equiv& x_1 - x_p & G_p\sin\beta_p &\equiv& y_1 - y_p \\ G_c\cos\beta_c &\equiv& x_2 - x_c & G_c\sin\beta_c &\equiv& y_2 - y_c \end{array}$$

Thus, we have

$$\begin{array}{rclcrcl} x_\iota - x &=& F_\iota\cos\alpha_\iota - G_\iota\cos\beta_\iota &\Rightarrow& G_\iota\cos\beta_\iota &=& (x - x_\iota) + F_\iota\cos\alpha_\iota \\ y_\iota - y &=& F_\iota\sin\alpha_\iota - G_\iota\sin\beta_\iota &\Rightarrow& G_\iota\sin\beta_\iota &=& (y - y_\iota) + F_\iota\sin\alpha_\iota \end{array}$$

Now by the addition of the square of these two equations, we have the following relation:

$$(x - x_\iota)\cos\alpha_\iota + (y - y_\iota)\sin\alpha_\iota = \mathcal{J}_\iota \equiv \frac{G_\iota{}^2 - F_\iota{}^2 - \mathcal{I}_\iota{}^2}{2F_\iota} \tag{17}$$

Now, using the relation $\sin\alpha_\iota = \pm\sqrt{1 - \cos^2\alpha_\iota}$, we obtain, after some manipulations, second order polynomial equations for $\cos\alpha_\iota$:

$$\cos^2\alpha_\iota - 2\left(\frac{x - x_\iota}{\mathcal{I}_\iota}\right)\frac{\mathcal{J}_\iota}{\mathcal{I}_\iota}\cos\alpha_\iota + \left(\frac{\mathcal{J}_\iota}{\mathcal{I}_\iota}\right)^2 - \left(\frac{y - y_\iota}{\mathcal{I}_\iota}\right)^2 = 0 \tag{18}$$

Finally, we obtain (using definition of α_ι to chose signs of solutions)

$$\cos\alpha_\iota = \frac{(x - x_\iota)}{\mathcal{I}_\iota}\frac{\mathcal{J}_\iota}{\mathcal{I}_\iota}\left\{1 + \sqrt{1 + \left(\frac{\mathcal{I}_\iota}{x - x_\iota}\right)^2\left[\left(\frac{y - y_\iota}{\mathcal{J}_\iota}\right)^2 - 1\right]}\right\} \tag{19}$$

and by symmetry of equations (17)

$$\sin\alpha_\iota = \frac{(y - y_\iota)}{\mathcal{I}_\iota}\frac{\mathcal{J}_\iota}{\mathcal{I}_\iota}\left\{1 + \sqrt{1 + \left(\frac{\mathcal{I}_\iota}{y - y_\iota}\right)^2\left[\left(\frac{x - x_\iota}{\mathcal{J}_\iota}\right)^2 - 1\right]}\right\} \tag{20}$$

Remark: With the figure, we see that $\mathrm{sign}(x_1 - x) = \mathrm{sign}(x - x_p)$ *and* $\mathrm{sign}(x_2 - x) = \mathrm{sign}(x - x_c)$, *hence the non ambiguity in choice of signs. The same applies to equations with* $\sin\alpha_\iota$.

[6] For simplicity, we will not write the (x, y) dependence of the functions.

2.2.2 Results and conclusion

We have α_ι depending on the data of the problem and coordinates (x, y) - See Eq. (19). Now we are able to determine x_1, y_1, x_2, y_2 which depend only of position of P, C and B.

In the case where the projected grating pattern is periodic along the x-axis, we have $I_0(x, y) \equiv I_0(x)$, that is to say

$$I(x_2, y_2) = I_0(x_1) \qquad \Rightarrow \qquad I(x + f(x, y), y + g(x, y)) = I_0(x + h(x, y))$$

where $f = F_c \cos\alpha_c$, $g = F_c \sin\alpha_c$ and $h = F_p \cos\alpha_p$; we assume $r = 1$. Now equation (12) becomes

$$I(x, y) = I_0\Big[x - f(x, y) + h\big[x - f(x, y), y - g(x, y)\big]\Big] \equiv I_0(x + \delta x(x, y)) \tag{21}$$

and $\Delta\phi = 2\pi f_0 \delta x$, *cf.* equation (10).

It is now necessary to see whether it is viable to take square roots such as in equations (19) and (20). Using the definition of $\mathcal{J}_\iota$ given in (17) we obtain:

$$\mathcal{J}_\iota = \frac{1}{2}\frac{h}{z_\iota - s}\left(\left(\frac{z_\iota}{s}\right)^2 - \left(\frac{z_\iota - s}{s}\right)^2 - 1\right)\mathcal{I}_\iota \tag{22}$$

We note $\varepsilon_\iota \equiv s/z_\iota$ and assuming $|\varepsilon_\iota| \ll 1$, we have

$$\mathcal{J}_\iota = \mathcal{I}_\iota\left(1 - {\varepsilon_\iota}^2\right) + \mathcal{O}\big({\varepsilon_\iota}^3\big)$$

which justify the existence of solutions (19) and (20) in the limit $\varepsilon_\iota \ll 1$.

Remark: $\mathcal{O}({\varepsilon_\iota}^n)$ denote Landau notation when $\varepsilon_\iota \to 0$.

2.2.3 Relationship between the phase and the amplitude of the signal

In the following, we suppose that $|\varepsilon_\iota| \ll 1$ and $I_0(x, y) = I_0(x)$. By previous discussion,

$$\frac{\Delta\phi}{2\pi f_0} = \delta x = -f(x, y) + h\big[x - f(x, y), y - g(x, y)\big] \tag{23}$$

Thanks to the definition of F_ι and equations (19) and (20), considering only the first order terms in ε_ι, we have $F_\iota = \varepsilon_\iota \mathcal{I}_\iota + \mathcal{O}(\varepsilon_\iota)$ and

$$\cos\alpha_\iota = \frac{x - x_\iota}{\mathcal{I}_\iota} + \mathcal{O}(\varepsilon_\iota) \quad \text{ and } \quad \sin\alpha_\iota = \frac{y - y_\iota}{\mathcal{I}_\iota} + \mathcal{O}(\varepsilon_\iota)$$

Finally, equation (23) becomes

$$\frac{\Delta\phi}{2\pi f_0} = \varepsilon_p(x - x_p) - \varepsilon_c(x - x_c) + \mathcal{O}\big(\varepsilon_p^3\big) + \mathcal{O}\big(\varepsilon_c^3\big) \tag{24}$$

and therefore,

$$s(x, y) \underset{\varepsilon_\iota \to 0}{\sim} \frac{\Delta\phi}{2\pi f_0}\left(\frac{x - x_p}{z_p} - \frac{x - x_c}{z_c}\right)^{-1} \tag{25}$$

2.2.4 To go further

If the LCD panel of the projector has an angle of θ relative to a normal plane of the surface and is parallel to the fringes of the grating pattern, we can show that (see for example [16, 17]) $\Delta\phi \to \Delta\phi' = \Delta\phi\cos\theta$ and $I_0 \to I_0' = \sum A_n' \exp(inkx\cos\theta)$ with

$$\frac{A_n'}{A_n} = \exp\left(-2nkx\cos\theta\sin^2\theta\frac{x}{x_c - x_p}\right)$$

Also, by symmetry (Fermat principle), the same conclusion can be made if it is instead the camera which has an angle of θ relative to the surface: $\Delta\phi \to \Delta\phi'$ and $I_0 \to I_0'$.

In the case where the LCD panel is not parallel to the fringes (or whether the projected image is not parallel to the fringes), we lose symmetry but we keep periodicity in the x-direction: $I_0(x, y) \neq I_0(x)$. Thus, we must consider Eq. (21) and introduce a second angle ϑ relative to the normal of the other direction.

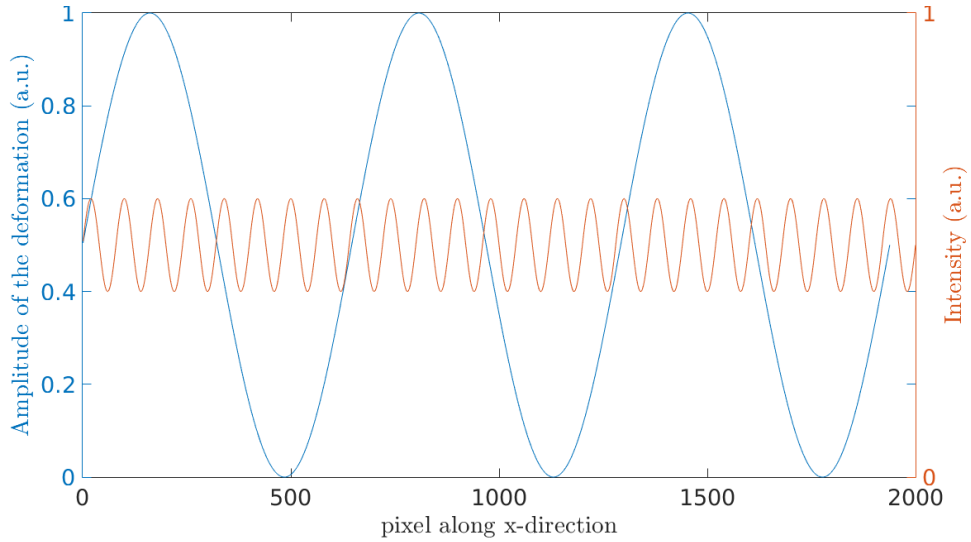

Figure 4: Example of used deformation and intensity in the analyse. We have been representing a sinusoidal deformation with frequency 3 $(1938\text{px})^{-1}$ and intensity of the sinusoidal pattern with frequency 25 $(1938\text{px})^{-1}$ along x-direction.

Note about uncertainty of ΔZ

After some manipulation on equation (25), we find for some deformation s:

$$\frac{z_p}{z_c} = \left((x - x_p) - \frac{\Delta\phi(x,y)}{s(x,y)}\frac{z_p}{2\pi f_0}\right)(x - x_c)^{-1} \equiv \Lambda^{-1}$$

where Λ is constant. Hence

$$\Delta Z \equiv z_p - z_c = z_p(1 - \Lambda) \tag{26}$$

Remark: To know z_p we measure the size of the projection on the screen as we know the angle of the projector lens.

Note about uncertainty of ΔY

Assuming $y_p \neq y_c$, we note $\Delta Y \equiv y_p - y_c$. Thus this effect introduce correcting terms in $\mathcal{O}\left({\varepsilon_\iota}^3\right)$ in equation (24). If $\Delta Y \ll {\varepsilon_\iota}^{-1}$, we can neglect this effect for calculations.

2.3 Parameter search

The aim of the parameter search was to find the optimum combination of parameters to obtain the most accurate 3D reconstruction of the measured object. As well as what resulting errors occur if there is any deviation from these optimum values.

In this study, we use a sinusoidal signal along the x-direction (see figure 4). Thus to find the amplitude using the profilometry method (*cf.* section 2.1), we take the Fourier transform of the reconstructed surface along x-direction and, depending on the effectiveness of the method, its spectrum is composed of only of one harmonic (by mathematical definition of the Fourier transform). The spectrum of the reconstructed deformed surface is an indication of the quality of the reconstruction using the method. By this way, we can check the quality of the reconstruction with the sum of the amplitudes of each harmonic (without the first): a perfect sinusoid will have only one harmonic in its Fourier spectrum and this sum should be null.

2.3.1 Parameters to be measured

The parameters we consider are:

- The distance between the camera and projector in the x, y and z direction.
- The distance between the camera and the surface (z-direction).
- The pixel size due to the camera (Similar to above, but can change if the resolution of the camera is increased).
- Frequency of the observed grating pattern. In the following, the frequencies will be expressed in unit u.f. $\equiv$ $(1938\text{px})^{-1}$.
- Amplitude of the deformation to be measured.

– Number of pixels per cycle of the grating pattern (*i.e.* the sinusoidal quality of the pattern).

For the real images, the potential error sources could be result of several contributions. For instance the reflexivity r of the surface (*cf.* equation (10)), which we assume equal to 1, or the imperfect optical alignment and focusing of the lenses, Gauss distortion etc.

2.3.2 The parameter search process

As our MATLAB code was able to generate images and automatically process them using FTP, we were able to let it run and obtain data for hundreds of different parameter values.

The first variable to be considered was the distance between the camera and projector, denoted by x_c - the x-coordinate of the camera. The actual distance between the camera and projector is given by $d = x_c - x_p$, but as we set $x_p = 0$ by default, we can just use x_c. We varied this value from 0.1 m to 1 m in steps of 0.005 m to obtain 181 data points (arbitrary), while keeping fixed values for the following (again, arbitrary):

– Distance between camera and projector in y and z directions, $z_c = z_p$, $y_c = y_p$.
– Distance between camera and the surface, $z_c = 1.75$ m.
– Pixel size, l_{px}. This depends on the resolution of the camera in the x-direction R_x, the angle of the camera lens in the x-direction C_x, and z_c, given by the following:

$$l_{\text{px}} = \frac{z_c}{R_x/2} \tan\left(\frac{C_x}{2}\right)$$

The values we set for R_x and C_θ were based on the specifications of our laboratory camera, $R_x = 1938$ and $C_x = 66°$. Which gives a corresponding pixel size of 1.24 mm.
– Observed frequency pattern, $f_0 = 100$.
– Amplitude of the object to be measured, $A = 0.01$ mm.
– The type of the object we used was a sine wave, which covered the surface (height and width) of our image. It had a period such that three wavelengths covered the width of the image, that is to say with frequency equal to 3 u.f.. The position of the wave was such that it was parallel to the width of the image.
– The number of pixels per cycle N_x of the grating pattern is dependent on the observed grating frequency, the relationship is given by,

$$N_x = \frac{R_x}{f_0}$$

It should be noted that this only gives the average number of pixels per cycle. This is due to the discretisation of the sin-wave pattern, unless $N_x \to \infty$, we cannot construct a perfect sinusoidal pattern. Thus for a low value of N_x, there will be a variance in each constructed wavelength, which causes a variance in the number of points per cycle.

We then ran the simulation for $x_c = 0.1 \to 1$ m again for different fixed values of the object amplitude[7], the distance between the camera and screen[8] and the observed grating frequency[9].

The next step was to change the variable z_c, which we changed from 0.2 m to 5 m and used the MATLAB function `linspace` such that we had 850 data points. Again we kept the other parameters fixed as before, now with $x_c = 0.5$ m. However, with changing z_c, there will be a change in the pixel size as R_x is a fixed value. We did not implement a compensatory change of R_x to keep the pixel size constant, as we wanted to represent our laboratory set-up, and it would of resulted in generating images of a very high pixel size.

Again, as before, we then ran the code again for $z_c = 0.1 \to 5$ m, for different fixed values of the object amplitude[7], the observed grating frequency[9] and the distance between the camera and projector[10].

Finally we ran the code for changes in the observed grating frequency, for values of $f_0 = 50 \to 900$ u.f. in intervals of 1, generating 850 data points. We kept the other parameters fixed at the values mentioned above. We then ran the code again altering these fixed values.

As with z_c, altering f_0 changes another variable, in this case the other variable affected is the average number of pixels per cycle N_x. An increase of f_0 will decrease the number of pixels per cycle, and so to keep N_x constant, it is necessary to change R_x for each change in f_0. However, as shown later, the accuracy of the reconstructed object using FTP is much more dependent on values of f_0 than the integrity of the sinusoidal grating pattern (indicated by N_x). This means keeping N_x fixed while altering f_0 only has a very small effect on the reconstruction, and thus we can allow N_x to vary (decrease) and still obtain reliable data for changes

[7] $A = 0.01,\ 0.02,\ 0.05,\ 0.1,\ 0.2,\ 0.5,\ 1,\ 2$ and 5 mm.
[8] $z_c = 1,\ 1.25,\ 1.5,\ 1.75$ and 2 m.
[9] $f_0 = 50,\ 75,\ 100,\ 125,\ 150,\ 175,\ 200$ u.f..
[10] $x_c = 0.1,\ 0.28,\ 0.46,\ 0.64,\ 0.82$ and 1 m

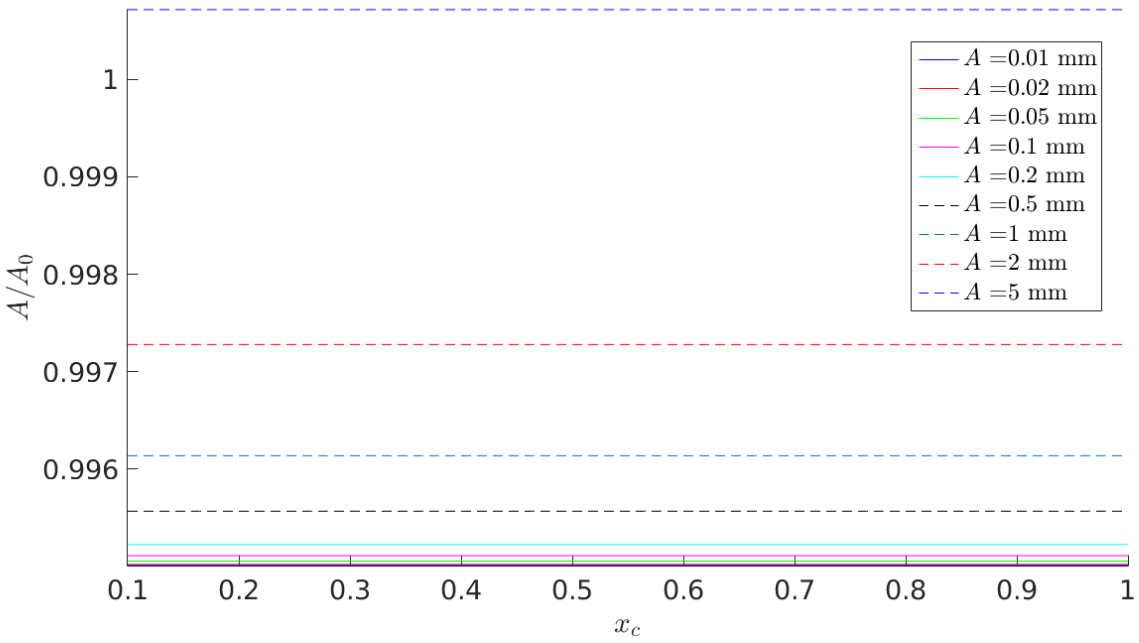

Figure 5: Reconstructed amplitude A divided by the input amplitude A_0 in function of the distance between the projector and the camera along the x-direction x_c. This graph is for a configuration with $f0 = 200$ u.f. and $z_c = 1.75$ m; the frequency of the deformation is 3 u.f..

in f_0 up to values of $f_0 = 200$ u.f.. In fact, the same argument can be made for the change in pixel size for a change in z_c.

Using the data obtained by manipulating these three variables, we can gain insight into what could be an optimum combination of x_c, z_c and f_0 for a specific object amplitude A. However, these results will have been constructed in the ideal case of $y_c = y_p$ and $z_c = z_p$. In reality it will not be possible to obtain a set-up where this is true, so it is necessary to see the resulting error for $y_c \neq y_p$ and $z_c \neq z_p$ and apply necessary corrections.

2.4 Results

It appears that the accuracy of the method is not dependent on the distance between the camera and the projector along the x-direction (see figure 5). For an amplitude of the deformation varying from 0.01 mm to 5 mm, we have obtained an amplitude reconstructed by the FTP method near the input amplitude to construct the image with a relative error less than 1% and this on the complete variation set of the other variables[8,9].

Then, it appears that the number of points per cycle is not relevant for the accuracy of the method. As shown in figure 6, the precision on the reconstructed amplitude converges logarithmically to the best values when we increase the frequency of the pattern. We note a limiting frequency for which the reconstruction is stochastic and inaccurate (see figure 7). This frequency correspond approximatively to when the number of points per cycle is 2 (2.3 exactly); beyond this frequency, the pixelisation of camera breaks the periodicity of the pattern. Once again we have obtained these results on the complete variation set of the other variables. Besides, we have done the same work for several frequencies of the deformation, and we have obtained exactly the following results: the accuracy of the method does not depend on the ratio between frequency of the pattern and the frequency of the deformation[11].

> *Remark: We have obtained the same results with a square pattern. Actually, if we use a non-sinusoidal pattern as a square pattern, the Fourier space of the decomposition is composed of several harmonics. Each harmonic contains the same information on the deformation of the free surface, that is to say phi. Strictly speaking, take the n-th harmonic is equivalent to take the first and the method should have in principle the same accuracy in both cases.*

In the figure 8, we have represented the reconstructed amplitude as a function of the distance between the camera and the free surface z_c. To construct this graph, we have kept constant the number of points per cycle on the pattern and on the deformation, so that z_c is proportional to the pixel size but the ratios $l_{\text{px}}/(1/f_0)$ and $l_{\text{px}}/(1/N)$ are kept. Strictly speaking, all the images are homothetic and only the ratio $\varepsilon \equiv A_0/z_c$, where A_0 is the input amplitude, is varied. This figure show the importance to be in a configuration with $A \ll z_\iota$.

[11] Of course, accuracy of the method is limited by the ratio between the pixels size and the frequency of the deformation: if the pixels size is bigger than typically size of the deformation, we cannot detect the details.

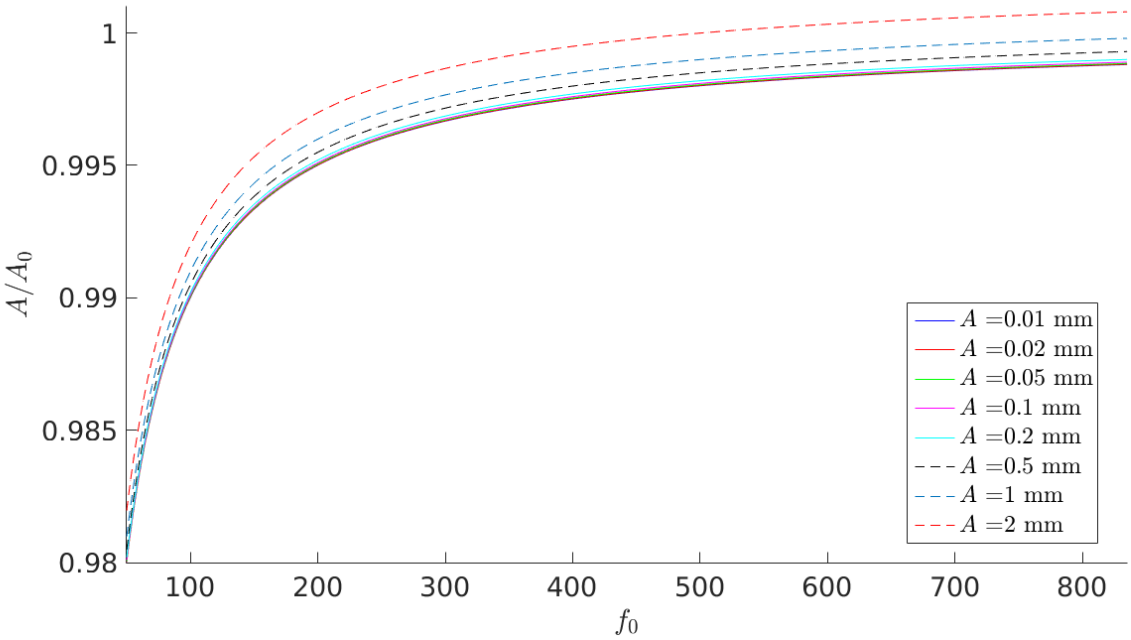

Figure 6: Reconstructed amplitude A divided by the input amplitude A_0 in function of the frequency of the pattern f_0. This graph is for a configuration with $x_c = 0.1$ m and $z_c = 2$ m; the frequency of the deformation is 3 u.f..

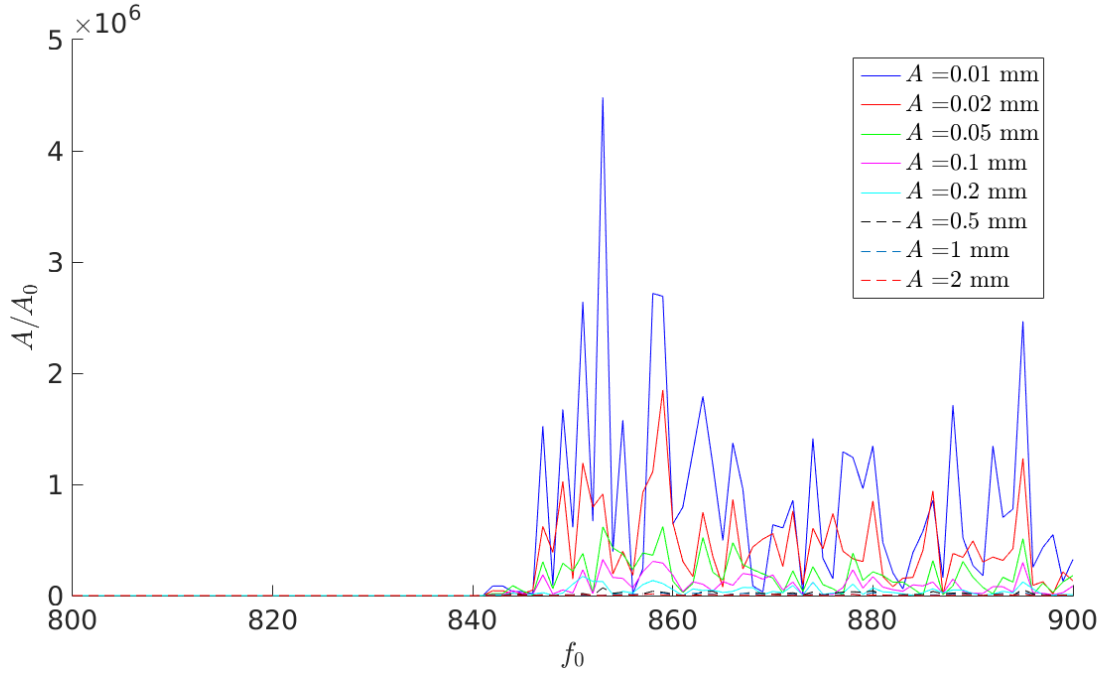

Figure 7: Reconstructed amplitude A divided by the input amplitude A_0 in function of the frequency of the pattern f_0. This graph is for a configuration with $x_c = 0.1$ m and $z_c = 2$ m; the frequency of the deformation is 3 u.f.. We observe a limit frequency ($f_0 = 840$) corresponding to 2 pixels per cycle. Note that the result of the reconstruction diverges more for the small amplitudes

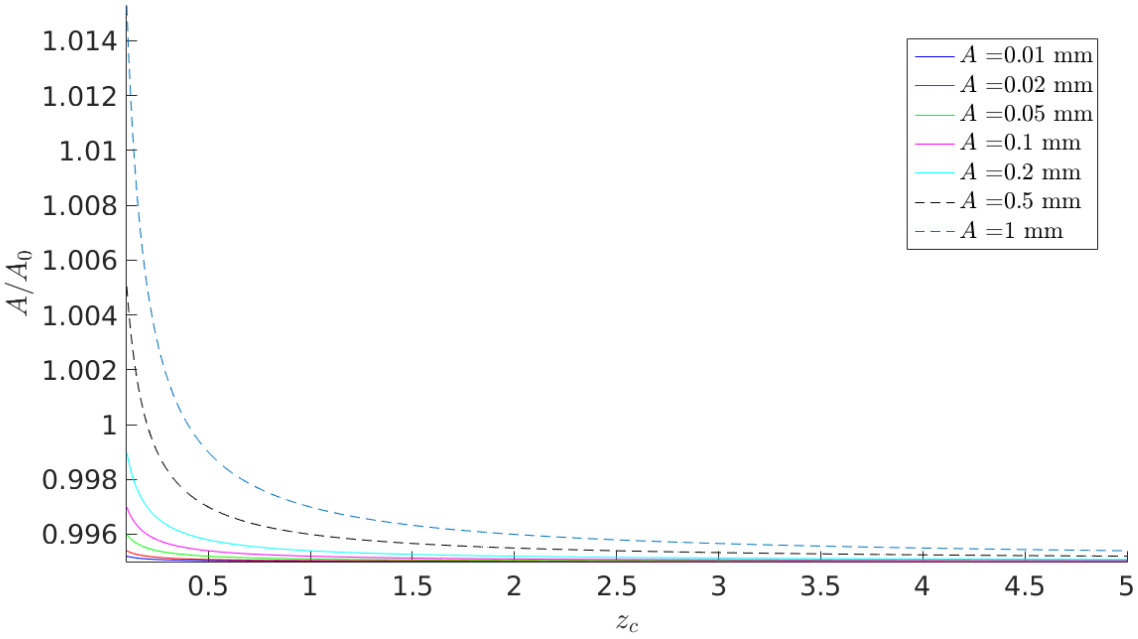

Figure 8: Reconstructed amplitude A divided by the input amplitude A_0 in function of the distance between the camera and the free surface z_c. This graph is for a configuration with $f_0 = 200$ u.f. and $x_c = 0.1$ m; the frequency of the deformation is 3 u.f..

Note about ε approximation

To construct images and find the relationship between the phase and the amplitude (see equation (24), we consider only the fist order in $\varepsilon \equiv A_0/z_c$ where A_0 is the input amplitude. Thus we have a process to plot the reconstructed amplitude as a function of ε, keeping the other variables constant. We have found exactly the same results for each set of parameters[8,10] (see figure 9). It seems that the reconstructed amplitude can be expressed, to good approximation, as the following:

$$A \equiv A_0 \left(p(f_0) + q(f_0)\varepsilon\right) = A_0 \left(p(f_0) + q(f_0)\frac{A_0}{z_c}\right) \tag{27}$$

where $p(f_0)$ and $q(f_0)$ are functions of f_0.

These results are in agreement with the approximation, and explain the shift between the curves of different amplitudes appearing in figures 5, 6 and 8.

Then, we have done the same study varying distance between the camera and the free surface z_c, keeping the ratio ε constant. We have obtained zero dependence on the accuracy (see figure 10). Now, we can write the reconstructed amplitude as the following:

$$A \equiv A_0 w(\varepsilon, f_0) \tag{28}$$

where $w(\varepsilon, f_0)$ is a function of ε and f_0. Hence,

$$w(\varepsilon, f_0) = p(f_0) + q(f_0)\varepsilon \tag{29}$$

The functions $p(f_0)$ and $q(f_0)$ are given in figure 11. We have found,

$$p = \frac{q}{2} = 1 - \frac{1}{f_0}$$

Finally, adding this relationship to the method to correct for deviations because of the ε approximation, we should obtain optimal results on the accuracy of the FTP method.

Conclusion

Finally, we have argued that it was possible to reproduce, in laboratory, analogue fluid systems which should permit us to study some of the peculiar physics related to black holes. Considering hydrodynamic equations, we find that sound waves in classical fluids obey to the same equation of motion than the photons near the black holes.

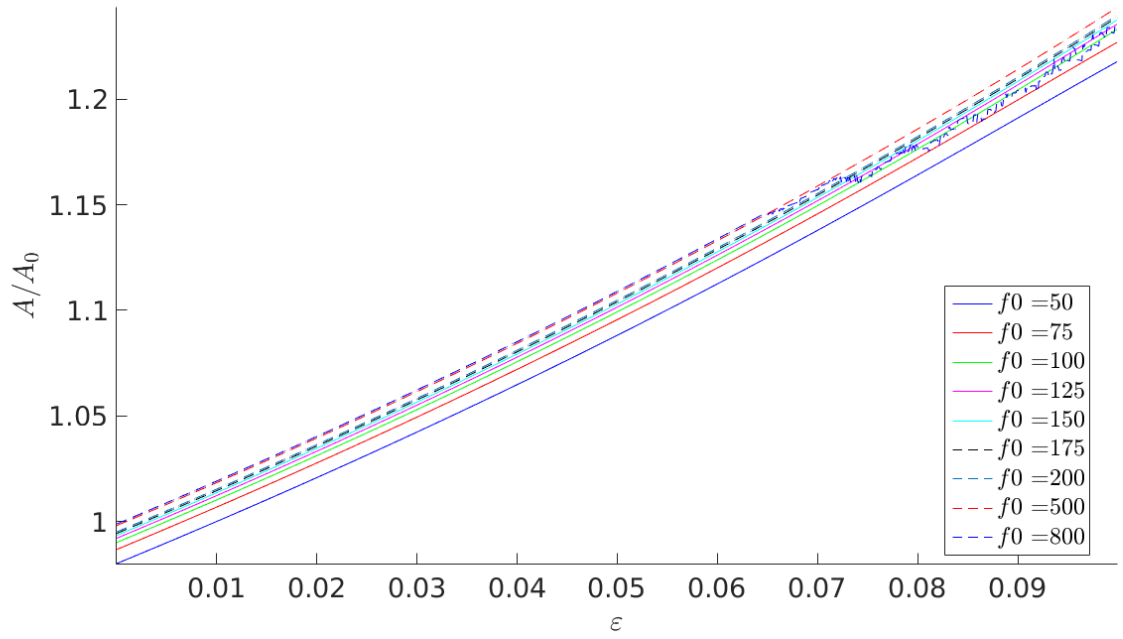

Figure 9: Reconstructed amplitude A divided by the input amplitude A_0 in function of ε. The parameter x_c and z_c are not specified because no deviation is found between each set of this parameter.

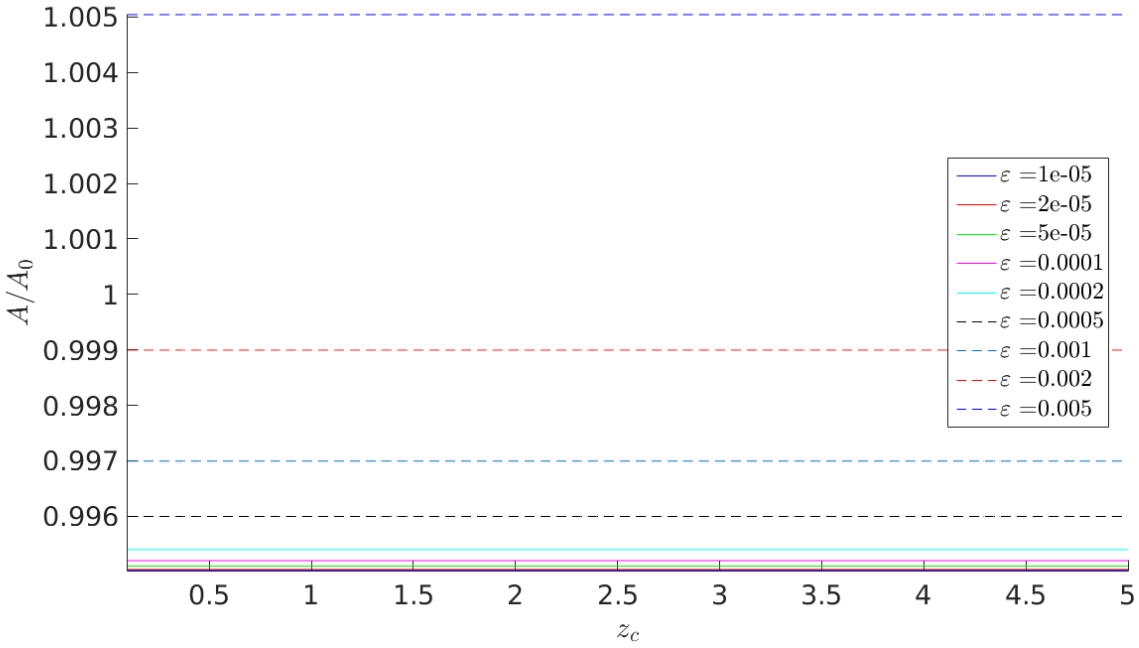

Figure 10: Reconstructed amplitude A divided by the input amplitude A_0 in function of z_c for several values of ε ($f_0 = 200$ u.f.). The parameter x_c is not specified because no deviation is found between each set of this parameter.

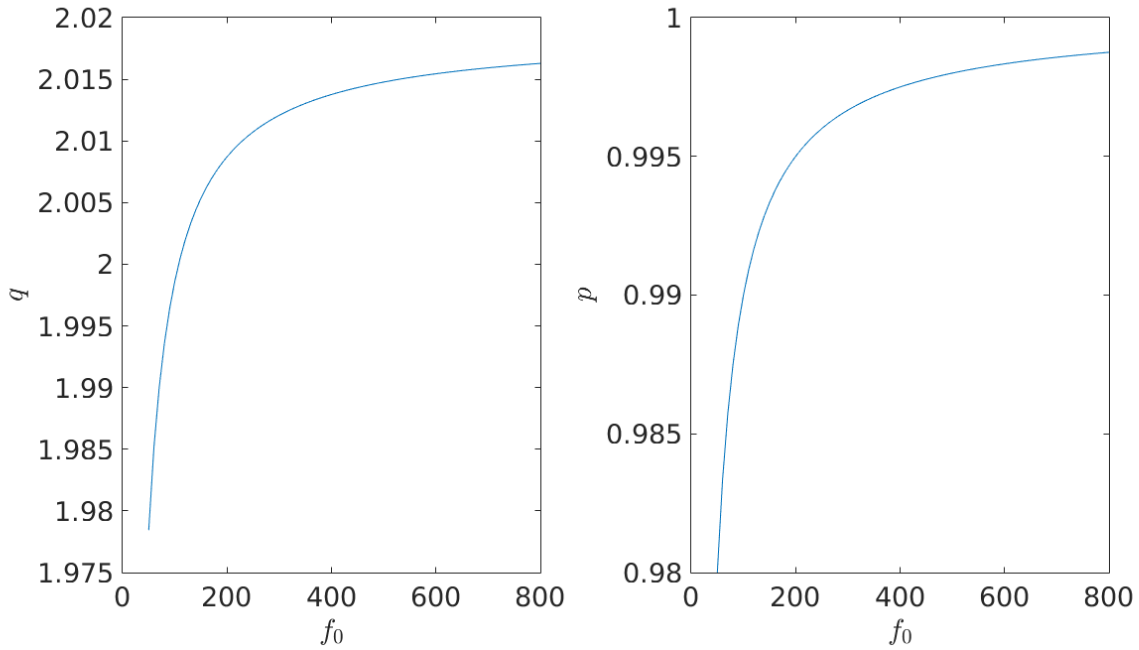

Figure 11: The functions p and q such as $A = A_0\,(p + q\varepsilon)$.

We have presented a method to measure wave deformation on the water surface based on the Fourier transform profilometry. We project a periodic pattern on the water surface and the deformation modulate the phase of the signal. This modulation is linked to the amplitude deformations so that this method permit us to measure supperradiant scattering.

This internship was devoted to develop and improve the FTP method. We first used ray-tracing methods to numerically simulate the deformation of a given grating pattern on deformed surfaces, we have then used these to test and analyse the method. We have obtained, on the one hand, the accuracy has no dependence on the distance between the camera and the projector. On the other hand, better results using can be obtained by increasing the grating frequency (which is limited by two pixels per cycle); and increasing the distance between the camera and the free surface. Last but not least, we studied the implication of the approximation assuming that the deformation is small compared to the distance between the camera and the free surface.

Our key finding of our study of the FTP method is, that it is not limited by the pixel size at the free surface, as for example stated in [18]. The key factors are frequency of the pattern. For instance we could resolve a sin-wave with an amplitude of 0.01 mm with a relative error of 0.1%, while the pixel size on the free surface was 1.24 mm.

Then, the next steps are to apply our improved method to, first the solid surfaces and then the air-water interfaces.

A Demonstration of ray-tracing method

A.1 Proposition

We propose to demonstrate the relation (12)

$$I(x_2, y_2) \propto I_0(x_1, y_1)$$

A.2 Definitions

In the following, we consider a monochromatic and incoherent light. We introduce some useful quantities for a source with area d^2S and with coordinate $\boldsymbol{X}$ (*cf.* figure 12 for notations)[12]:

– The radiance L (of the elementary source)

$$\mathrm{d}^4\phi(\boldsymbol{X}, \boldsymbol{u}) \equiv L(\boldsymbol{X}, \boldsymbol{u}) \cos\theta \, \mathrm{d}^2S \, \mathrm{d}^2\Omega \tag{A.1}$$

where $\mathrm{d}^4\phi$ is the elementary energy flow emitted by d^2S in the elementary solid angle $\mathrm{d}^2\Omega$ centred around $\boldsymbol{u}$; $\hat{\boldsymbol{n}} \cdot \boldsymbol{u} = \cos\theta$ where $\hat{\boldsymbol{n}}$ is the unitary normal vector to the surface d^2S. In this definition, the quantity d^2S correspond to area of the source where radiance L can be considered constant.

> *Remark: In the following we suppose the energy can be considered diffused isotropically by several contributions: the absorption-diffusion process of the surfaces, microscopic deformations (granularity) of the surfaces, etc. In other words, we suppose without loss of generality and for simplicity that the surface (water) is an ideal diffuse surface: Lambert's cosine law is available in this case. Same consideration for the LCD panels of the projector and the camera. For these systems, the radiance $L(\boldsymbol{X}, \boldsymbol{u}) \equiv L(\boldsymbol{X})$ is isotropic.*

– The intensity $\tilde{I}$ (of the elementary source)

$$\mathrm{d}^4\phi(\boldsymbol{X}, \boldsymbol{u}) \equiv \mathrm{d}^2\tilde{I}(\boldsymbol{X}, \boldsymbol{u})\mathrm{d}^2\Omega \tag{A.2}$$

> *Remark: For lambertian source, $\mathrm{d}^2\tilde{I}(\boldsymbol{X}, \boldsymbol{u}) = \mathrm{d}^2\tilde{I}_0(\boldsymbol{X}) \cos\theta$ where $\mathrm{d}^2\tilde{I}_0(\boldsymbol{X}, \boldsymbol{u}) = L(\boldsymbol{X}, \boldsymbol{u}) \, \mathrm{d}^2S$.*

– The irradiance E (of an elementary surface by the elementary source)

$$\mathrm{d}^6E(\boldsymbol{X}, \boldsymbol{u}) \equiv \mathrm{d}^4\phi(\boldsymbol{X}, \boldsymbol{u}, \Omega) \, \mathrm{d}^2S' \tag{A.3}$$

where d^2S' is the elementary surface intercepted by $\mathrm{d}^2\Omega$ (centred at $\boldsymbol{X}$) in $\boldsymbol{u}$ direction.

We can write the irradiance like:

$$\mathrm{d}^6E(\boldsymbol{X}, \boldsymbol{u}) = L(\boldsymbol{X}, \boldsymbol{u}) \cos\theta \, \mathrm{d}^2S \, \mathrm{d}^2S' \, \mathrm{d}^2\Omega \qquad \text{where} \qquad \mathrm{d}^2\Omega = \frac{\cos\theta'}{d^2} \, \mathrm{d}^2S'$$

with d the distance between the elementary source and the elementary surface; $\hat{\boldsymbol{n}'} \cdot \boldsymbol{u} = -\cos\theta'$ where $\hat{\boldsymbol{n}'}$ is the unitary normal vector to the surface d^2S', *cf.* figure 12. Hence

$$\begin{aligned} \mathrm{d}^4\phi(\boldsymbol{X}, \boldsymbol{u}) &= L(\boldsymbol{X}, \boldsymbol{u}) \cos\theta \, \mathrm{d}^2S \, \mathrm{d}^2\Omega \qquad \text{where} \qquad \mathrm{d}^2\Omega' = \frac{\cos\theta}{d^2} \, \mathrm{d}^2S \\ &= L(\boldsymbol{X}, \boldsymbol{u}) \cos\theta' \, \mathrm{d}^2S' \, \mathrm{d}^2\Omega' \end{aligned}$$

– The reflectance ρ of an elementary surface

$$\mathrm{d}^4\phi'(\boldsymbol{X'}, -\boldsymbol{u}) \equiv \rho(\boldsymbol{X'}, \boldsymbol{u}) \, \mathrm{d}^2\phi(\boldsymbol{X}, \boldsymbol{u}) \tag{A.4}$$

where $\boldsymbol{X'}$ denote coordinate of the surface which receive the flow come from the source with coordinate $\boldsymbol{X}$ and $\mathrm{d}^4\phi'$ is emitted the flow by the elementary surface in the solid angle $\mathrm{d}^2\Omega'$ (centred at $\boldsymbol{X'}$) in $-\boldsymbol{u}$ direction.

[12] *e.g.* see the optic lectures of Jérôme Leygnier (in french), M1 of fundamental physics, Paris-Sud university.

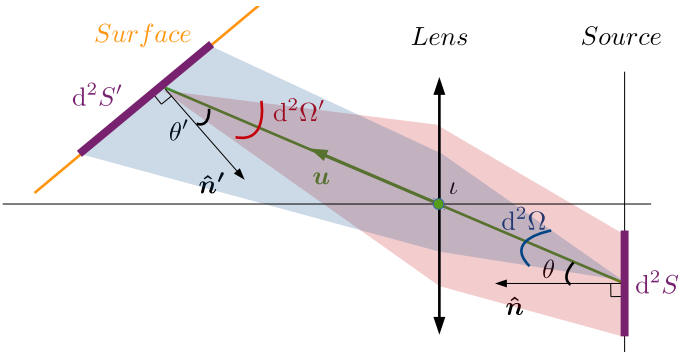

Figure 12: Notations. In the case where we consider the rays come from ι ($\iota = p, c \leftrightarrow i = 1, 2$), we define $\theta \equiv \delta_\iota$, $\theta' \equiv \gamma_\iota$ and $\Omega \equiv \mathrm{d}\Omega$; $\mathrm{d}^2S \equiv \mathrm{d}x_\iota\,\mathrm{d}y_\iota$; $\mathrm{d}^2S' \equiv \mathrm{d}x_i\,\mathrm{d}y_i$ and $\Omega' \equiv \mathrm{d}\Omega_\iota$ if we consider that the reference plan is the sensor; $\mathrm{d}^2S \equiv \mathrm{d}x_\iota\,\mathrm{d}y_\iota$, $\mathrm{d}^2S' \equiv \mathrm{d}^2\sigma_\iota$ and $\Omega' \equiv \mathrm{d}\Omega^0_\iota$ if we consider that the deformed surface is the sensor.

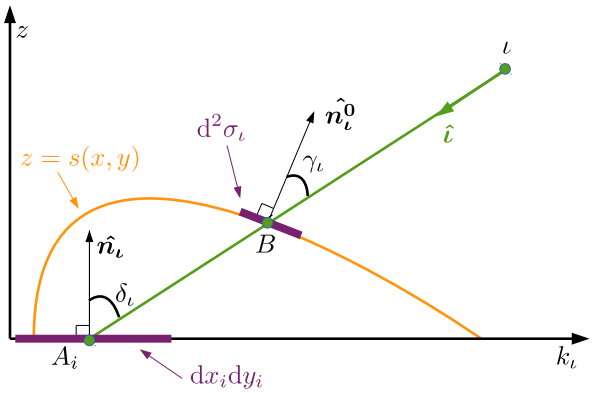

Figure 13: Notations. We introduce angles δ_ι and γ_ι, the elementary surfaces $\mathrm{d}^2\sigma_\iota$ and $\mathrm{d}x_i\,\mathrm{d}y_i$ ($\iota = p, c \leftrightarrow i = 1, 2$).

A.3 Demonstration

Do not forget that the camera and the projector are optical systems where we noted C and P the center of there convergent lenses. Thus $\mathrm{d}^2\Omega$ centred around the elementary area $\mathrm{d}^2S' \equiv \mathrm{d}x_\iota\,\mathrm{d}y_\iota$ of the LCD panel of ι correspond to an elementary area on the lens of ι. Then, in previous relation of the flow, $\mathrm{d}^2\Omega'$ correspond to the solid angle enlightening the area of the lens which correspond to an surface $\mathrm{d}^2S \equiv \mathrm{d}x_\iota\,\mathrm{d}y_\iota$ on the LCD panel (*cf.* figure 12).

For $\mathrm{d}^2\Omega$ fixed, we define elementary surfaces $\mathrm{d}^2S' \equiv \mathrm{d}x_i\,\mathrm{d}y_i$ ($i = 1, 2 \leftrightarrow \iota = p, c$) and $\mathrm{d}^2\sigma_\iota$ on the flat surface and the deformed surface respectively intercepted by this solid angle.

Now, we define the solid angles $\mathrm{d}^2\Omega_\iota$ and $\mathrm{d}^2\Omega^0_\iota$ like the solid angles $\mathrm{d}^2\Omega'$ where associated elementary surfaces are noted $\mathrm{d}x_i\,\mathrm{d}y_i$ and $\mathrm{d}^2\sigma_\iota$ respectively, *cf.* equation (A.3). These two solid angles intercept the same surface $\mathrm{d}x_\iota\,\mathrm{d}y_\iota$ on the LCD panel of ι (*cf.* figure 12).

Then, we introduce the angles γ_ι and δ_ι with correspond to the angle θ' and defined by:

$$\hat{\boldsymbol{n}}_{\boldsymbol{\iota}} \cdot \hat{\boldsymbol{\iota}} = -\cos\delta_\iota \qquad\qquad \hat{\boldsymbol{n}}^{\boldsymbol{0}}_{\boldsymbol{\iota}} \cdot \hat{\boldsymbol{\iota}} = -\cos\gamma_\iota$$

where $\hat{\boldsymbol{n}}_{\boldsymbol{\iota}}$ and $\hat{\boldsymbol{n}}^{\boldsymbol{0}}_{\boldsymbol{\iota}}$ are the unitary vectors normal to the elementary surfaces $\mathrm{d}x_i\,\mathrm{d}y_i$ and $\mathrm{d}^2\sigma_\iota$ respectively; $\hat{\boldsymbol{\iota}}$ is the unitary vector directed by $\boldsymbol{\iota B}$ (*cf.* figure 13).

Using this notations, the flow come from the LCD panel of the projector on the elementary surface is:

$$\begin{aligned}\mathrm{d}^4\phi(\boldsymbol{X_p}, \hat{\boldsymbol{p}}) &= L(\boldsymbol{X_p}, \hat{\boldsymbol{p}})\cos\gamma_p\,\mathrm{d}^2\sigma_p\,\mathrm{d}^2\Omega^0_p \\ &= L(\boldsymbol{X_p}, \hat{\boldsymbol{p}})\cos\delta_p\,\mathrm{d}x_1\,\mathrm{d}y_1\,\mathrm{d}^2\Omega_p\end{aligned}$$

where $\boldsymbol{X_p}$ denote coordinate of the elementary source on the LCD panel of the projector which correspond to coordinate of A_1 on the flat surface. As far as, we have

$$\begin{aligned}\mathrm{d}^4\phi(\boldsymbol{X_{p'}}, \hat{\boldsymbol{p}'}) &= L(\boldsymbol{X_{p'}}, \hat{\boldsymbol{p}'})\cos\gamma_{p'}\,\mathrm{d}^2\sigma_{p'}\mathrm{d}^2\Omega^0_{p'} \\ &= L(\boldsymbol{X_{p'}}, \hat{\boldsymbol{p}'})\cos\delta_{p'}\,\mathrm{d}x_2{}'\,\mathrm{d}y_2{}'\,\mathrm{d}^2\Omega_{p'}\end{aligned}$$

The prime denote the fact that we consider the rays come from P to A_2 in the solid angle $\mathrm{d}^2\Omega'$ which intercept the area $\mathrm{d}x'_2\,\mathrm{d}y'_2$ (or the rays come from C to A_1 in the solid angle $\mathrm{d}^2\Omega'$ which intercept the area $\mathrm{d}x'_1\,\mathrm{d}y'_1$ whether the prime index C), that is to say $\iota = p', c' \leftrightarrow i = 2, 1$.

Now, we introduce ρ^f and ρ^d, the reflectances of the flat and the deformed surface respectively defined like the ratio between the outgoing flow and the incoming flow. Therefore we can write the flow come from the flat and the deformed surface to the LCD panel of the camera; and, by definition of the reflectance, we have:

$$\begin{aligned}\mathrm{d}^4\phi(\boldsymbol{X_i}, -\hat{\boldsymbol{\iota}}) &= L^d(\boldsymbol{X}, -\hat{\boldsymbol{\iota}})\cos\gamma_\iota\,\mathrm{d}^2\sigma_\iota\,\mathrm{d}^2\Omega^0_\iota \\ &= L^f(\boldsymbol{X_i}, -\hat{\boldsymbol{\iota}})\cos\delta_\iota\,\mathrm{d}x_i\,\mathrm{d}y_i\,\mathrm{d}^2\Omega_\iota\end{aligned}$$

which are equivalent to, in case of lambertian sources

$$L^d(\boldsymbol{X}, -\hat{\boldsymbol{\iota}}) \equiv L^d(\boldsymbol{X}) = L^f(\boldsymbol{X_i}, -\hat{\boldsymbol{\iota}})\frac{\cos\delta_\iota}{\cos\gamma_\iota}\frac{\mathrm{d}^2\Omega_\iota}{\mathrm{d}^2\Omega^0_\iota}\frac{\mathrm{d}x_i\,\mathrm{d}y_i}{\mathrm{d}^2\sigma_\iota}$$

with $L^d(\boldsymbol{X}, -\hat{\boldsymbol{\iota}}) \equiv \rho^d L(\boldsymbol{X_p}, \hat{\boldsymbol{p}})$, $L^f(\boldsymbol{X_1}, -\hat{\boldsymbol{p}}) \equiv \rho^f L(\boldsymbol{X_p}, \hat{\boldsymbol{p}})$ and $L^f(\boldsymbol{X_2}, -\hat{\boldsymbol{c}}) \equiv \rho^f L(\boldsymbol{X_{p'}}, \hat{\boldsymbol{p}'})$; $\boldsymbol{X} \equiv (x, y, z = s)$ and $\boldsymbol{X_i} \equiv (x_i, y_i, z = \lambda)$.

> *Remark: In the case where sources are not lambertian, we can write $L^d(\boldsymbol{X}, -\hat{\boldsymbol{\iota}}) \equiv L^d(\boldsymbol{X})\delta_{\boldsymbol{X}}(\vartheta, \varphi)$ where $\delta_{\boldsymbol{X}}$ is the angular distribution of radiance in $\boldsymbol{X}$, $\hat{\boldsymbol{\iota}} \cdot \hat{\boldsymbol{e_z}} \equiv -\cos\vartheta$ and $\hat{\boldsymbol{\iota}} \cdot \hat{\boldsymbol{e_x}} \equiv -\cos\varphi$. As far as for the radiance L^f.*

Hence,

$$\begin{aligned}L^f(\boldsymbol{X_2}, -\hat{\boldsymbol{c}}) &= \left(\frac{\cos\gamma_c}{\cos\gamma_p}\frac{\cos\delta_p}{\cos\delta_{c'}}\frac{\mathrm{d}^2\Omega_p}{\mathrm{d}^2\Omega_c}\frac{\mathrm{d}^2\Omega^0_c}{\mathrm{d}^2\Omega^0_p}\frac{\mathrm{d}^2\sigma_c}{\mathrm{d}^2\sigma_p}\frac{\mathrm{d}x_1}{\mathrm{d}x'_1}\frac{\mathrm{d}y_1}{\mathrm{d}y'_1}\right)\left(\frac{\cos\delta_{c'}}{\cos\delta_c}\frac{\mathrm{d}x'_1}{\mathrm{d}x_2}\frac{\mathrm{d}y'_1}{\mathrm{d}y_2}\right)L^f(\boldsymbol{X_1}, -\hat{\boldsymbol{p}}) \\ &\equiv r(x, y)R(x, y)L^f(\boldsymbol{X_1}, -\hat{\boldsymbol{p}})\end{aligned}$$

Moreover in us case we have for lambertian sources

$$I_0(x_1, y_1) \equiv \mathrm{d}^2\tilde{I}(\boldsymbol{X_1}, -\hat{\boldsymbol{c}'}) = L^f(\boldsymbol{X_1}, -\hat{\boldsymbol{c}'})\,\mathrm{d}x'_1\,\mathrm{d}y'_1\cos\delta_{c'}$$

$$I(x_2, y_2) \equiv \mathrm{d}^2\tilde{I}(\boldsymbol{X_2}, -\hat{\boldsymbol{c}}) = L^f(\boldsymbol{X_2}, -\hat{\boldsymbol{c}})\,\mathrm{d}x_2\,\mathrm{d}y_2\cos\delta_c$$

and finally we obtain (*cf.* previous note for generality of discussion)

$$I(x_2, y_2) = r(x, y)I_0(x_1, y_1)$$

> *Remark: With evident notations, we have for non lambertian sources (*cf. *previous note for notations)*
>
> $$I(x_2, y_2) = r(x, y)\frac{\delta_{\boldsymbol{X_1}}(\vartheta_p, \varphi_p)}{\delta_{\boldsymbol{X_1}}(\vartheta_{c'}, \varphi_{c'})}\frac{\delta_{\boldsymbol{X}}(\vartheta_p, \varphi_p)}{\delta_{\boldsymbol{X}}(\vartheta_c, \varphi_c)}I_0(x_1, y_1)$$
>
> *with $\hat{\boldsymbol{\iota}} \cdot \hat{\boldsymbol{e_z}} \equiv -\cos\vartheta_\iota$ and $\hat{\boldsymbol{\iota}} \cdot \hat{\boldsymbol{e_x}} \equiv -\cos\varphi_\iota$ ($\iota = p, c \leftrightarrow i = 1, 2$ and $\iota = p', c' \leftrightarrow i = 2, 1$).*

References

[1] S. W. Hawking, "Black holes explosions?," *Nature* **248** (1974) 30–31. http://www.nature.com/nature/journal/v248/n5443/abs/248030a0.html. *cited page 2*

[2] S. Hawking, "Particle creation by black holes," *Communications in Mathematical Physics* **43** no. 3, (1975) 199–220. http://dx.doi.org/10.1007/BF02345020. *2 citations: pages 2 and 3*

[3] R. Parentani, "What did we learn from studying acoustic black holes?," *Int.J.Mod.Phys.* **A17** (2002) 2721–2726, arXiv:gr-qc/0204079 [gr-qc]. *cited page 2*

[4] T. Jacobson, "Black holes and Hawking radiation in spacetime and its analogues," *Lect.Notes Phys.* **870** (2013) 1–29, arXiv:1212.6821 [gr-qc]. *cited page 2*

[5] W. G. Unruh, "Experimental black-hole evaporation?," *Phys. Rev. Lett.* **46** (May, 1981) 1351–1353. http://link.aps.org/doi/10.1103/PhysRevLett.46.1351. *cited page 2*

[6] C. Misner, K. Thorne, and J. Wheeler, *Gravitation*. No. ptie. 3 in Gravitation. W. H. Freeman, 1973. *cited page 3*

[7] T. Jacobson, "Introduction to quantum fields in curved space-time and the Hawking effect," arXiv:gr-qc/0308048 [gr-qc]. *cited page 4*

[8] S. Weinfurtner, E. W. Tedford, M. C. Penrice, W. G. Unruh, and G. A. Lawrence, "Classical aspects of Hawking radiation verified in analogue gravity experiment," arXiv:1302.0375 [gr-qc]. *cited page 4*

[9] R. Schutzhold and W. G. Unruh, "Gravity wave analogs of black holes," *Phys.Rev.* **D66** (2002) 044019, arXiv:gr-qc/0205099 [gr-qc]. *cited page 4*

[10] M. Richartz, A. Prain, S. Weinfurtner, and S. Liberati, "Superradiant scattering of dispersive fields," *Class.Quant.Grav.* **30** (2013) 085009, arXiv:1208.3601 [gr-qc]. *cited page 5*

[11] M. Richartz, S. Weinfurtner, A. Penner, and W. Unruh, "General universal superradiant scattering," *Phys.Rev.* **D80** (2009) 124016, arXiv:0909.2317 [gr-qc]. *cited page 5*

[12] J. D. Bekenstein and M. Schiffer, "The Many faces of superradiance," *Phys.Rev.* **D58** (1998) 064014, arXiv:gr-qc/9803033 [gr-qc]. *cited page 5*

[13] M. Richartz, A. Prain, S. Liberati, and S. Weinfurtner, "Rotating black holes in a draining bathtub: superradiant scattering of gravity waves," *Phys.Rev.* **D91** no. 12, (2015) 124018, arXiv:1411.1662 [gr-qc]. *cited page 5*

[14] M. Takeda and K. Mutoh, "Fourier transform profilometry for the automatic measurement of 3-d object shapes," *Appl. Opt.* **22** no. 24, (Dec, 1983) 3977–3982. http://ao.osa.org/abstract.cfm?URI=ao-22-24-3977. *cited page 5*

[15] M. Takeda, H. Ina, and S. Kobayashi, "Fourier-transform method of fringe-pattern analysis for computer-based topography and interferometry," *J. Opt. Soc. Am.* **72** no. 1, (Jan, 1982) 156–160. http://www.osapublishing.org/abstract.cfm?URI=josa-72-1-156. *cited page 6*

[16] X. Mao, W. Chen, and X. Su, "Improved fourier-transform profilometry," *Appl. Opt.* **46** no. 5, (Feb, 2007) 664–668. http://ao.osa.org/abstract.cfm?URI=ao-46-5-664. *cited page 8*

[17] E. Zappa and G. Busca, "Fourier-transform profilometry calibration based on an exhaustive geometric model of the system," *Optics and Lasers in Engineering* **47** no. 7–8, (2009) 754 – 767. http://www.sciencedirect.com/science/article/pii/S0143816609000530. *cited page 8*

[18] P. Cobelli, A. Maurel, V. Pagneux, and P. Petitjeans, "Global measurement of water waves by fourier transform profilometry," *Experiments in Fluids* **46** no. 6, (2009) 1037–1047. http://dx.doi.org/10.1007/s00348-009-0611-z. *cited page 15*